NASA Technical Memorandum 100297

Finite Element Substructuring Methods for Composite Mechanics

(NASA-TM-100297) FINITE ELEMENT SUBSTRUCTURING METHODS FOR COMPOSITE MECHANICS (NASA) 17 p CSCL 11D

N88-17745

Unclas
G3/24 0125894

Pappu L.N. Murthy
Cleveland State University
Cleveland, Ohio

and

Christos C. Chamis
Lewis Research Center
Cleveland, Ohio

Prepared for the
International Conference on Composite Materials and Structures
sponsored by the India Institute of Technology at Madras
Madras, India, January 6–9, 1988

NASA

FINITE ELEMENT SUBSTRUCTURING METHODS FOR COMPOSITE MECHANICS

Pappu L.N. Murthy
Cleveland State University
Civil Engineering Department
Cleveland, Ohio 44115

Cristos C. Chamis
National Aeronautics and Space Administration
Lewis Research Center
Cleveland, Ohio 44135

SUMMARY

Finite element substructuring strategies to obtain numerical solutions for three typical problems of interest to the composites community, are presented in this paper. The key issue common to these problems is the presence of singular or near singular stress fields. The regions prone to see steep stress gradients, are substructured with progressively refined meshes to study the local response simultaneously with the global response. The results from the select examples indicate that finite element substructuring methods are computationally effective for composite singularity mechanics.

E-3946

INTRODUCTION

Finite element substructuring analysis has long been recognized as a viable alternative to analyze large scale structures. Efficient use of computer storage, reduction in computation time, and much less turnaround time are some of the advantages of finite element substructuring. Over the past few years, at the NASA Lewis Research Center, some of the solution capabilities available in MSC/NASTRAN have been utilized to analyze several problems related to composite structures (refs. 1 to 4). This research has focused on singular or near singular stress field behavior in composites. The approach has been to substructure the local regions with a progressively refined mesh and study the local response simultaneously with global response. The regions chosen for progressive refinement are near load application points, crack tip zones, and free edges. It is a well known fact that near-singular or singular stress fields exist in these regions. Experiences with the use of finite element substructuring solution strategies are described via three typical problems which represent current issues of interest in the composites community. However, the underlying solution principles are not limited to such problems only.

The selected problems are (1) impact and toughness characterization of composites using Charpy's impact test specimen, (2) free-edge stress analysis of composite laminates, and (3) fracture toughness predictions of composites for individual and combined fracture of modes I, II, and III. The objective of this paper is to report on the effectiveness of the finite element substructuring concept in conjunction with the analysis of structural composites with embedded singularities. Another important objective of the present study is to see how well one could relate the global response characteristics to the constituent level properties (fiber/matrix micromechanics) using two- and three-dimensional finite element analysis.

SELECT EXAMPLES

Impact and Toughness Characterization of Composites Using Charpy's Impact Test Specimen

Specimen geometry and finite element idealization. - The geometry of the standard Charpy test specimen (ASTM STD E23-7) along with the finite element idealization for smooth and notched specimens are shown in figure 1. Two finite element models of Charpy test specimens--one without a notch (smooth specimen) and one with a notch were selected for the present study. The material properties are assumed to be uniform, orthotropic, and obey a linear stress-strain law throughout the analysis. In addition, the specimen is assumed to be in a state of plane stress. The plane stress assumption is justified from the physics of the problem. The width restraints at the notch-tip are negligible because of the very low value of the respective Poisson's ratio. For the present analysis, the plane stress assumption implies that the stresses are permitted to vary along the specimen length and through the thickness but not across the width. This reduces the stress calculations to three; two normal and one shear.

With these assumptions, plane stress finite elements can be used to model the Charpy test specimen. For the smooth specimen all the elements are quadrilateral. The notched specimen is modeled with both triangular elements and quadrilateral elements. The triangular elements are used as transition elements in the areas around the supports, the load application point, and the notch. These are the regions where maximum stress concentrations are expected to occur and therefore are modeled with a finer mesh. The boundary conditions prescribed are such that the node at the left support is constrained from x, y, and z displacements, and the node at the right support is constrained from y and z displacements. In addition, for the notched specimen, three nodes closest to the right support are constrained from displacement in the y direction. The specimens are subjected to an impulse loading. The form of impact is a triangular function with a peak load of 2000 lb occurring at 500 μs of a total contact time of 1000 μs.

The details of the finite element models for the smooth and notched specimens are described in reference 1.

Finite element analysis method. - The MSC/NASTRAN general purpose structural analysis finite element computer program is used for the finite element analysis. The specific elements used are identified as CTRIA3 and CQUAD4. They are isoparametric elements. NASTRAN obtains the solution using a displacement formulation via rigid format solution sequence number 27. This solution sequence employs a direct time integration scheme to obtain the transient response of a structure subjected to impact.

The solution sequence number 27 of MSC/NASTRAN uses the integration algorithm based upon the Newmark Beta method (ref. 5). It provides stable results for the widest possible spectrum of practical problems without sacrificing either accuracy or efficiency. For complete details of the MSC/NASTRAN analysis, reference 6 should be consulted.

Composite system analyzed. - Flexural (Charpy-type) test specimens made from three typical composite systems are analyzed. They are T-300/Epoxy, Kevlar/Epoxy, and S-Glass/Epoxy composites. The specimens are all

unidirectional composites with the fibers parallel to the length (x-axis, fig. 1) of the specimen.

The plane stress-strain relationship (stiffness) coefficients required to input to NASTRAN are obtained by using the resident data-bank in the composite mechanics computer code ICAN (ref. 7).

Two types of load conditions are used in obtaining the results. The first is a static loading where a force of 2000 lb is applied at the center of the specimen on the top surface. The second is an impulse loading. This modeled as a triangular pulse with a peak value of 2000 lb in the middle. The pulse is modeled to last for 1000 μs. The transient response is, however, obtained for three contact time periods i.e., 3 μs.

Displacement and stress wave propagation. - The bulk wave and shear wave velocities are normally much higher compared to the flexural wave velocities. In order to capture the characteristics of propagation of these waves, a much smaller time step of integration (0.1 μs) is chosen. Figure 2 shows the dynamic displacement propagation in S-Glass/Epoxy, Kevlar/Epoxy, and T-300/Epoxy specimens. Two bulk wave velocity parameters and one shear wave velocity parameter are defined below to aid the following discussion of the displacement wave propagation results:

$$C_{B11} = \sqrt{\frac{G_{11}}{\rho}} \; ; \text{ where } G_{11} = \frac{E_{xx}}{1 - \nu_{xy}\nu_{yx}} \tag{1}$$

$$C_{B22} = \sqrt{\frac{G_{22}}{\rho}} \; ; \text{ where } G_{22} = \frac{E_{yy}}{1 - \nu_{xy}\nu_{yx}} \tag{2}$$

$$C_{S12} = \sqrt{\frac{G_{12}}{\rho}} \; ; \text{ where } G_{12} = G_{xy} \tag{3}$$

where ρ is the mass density of the material.

The velocities are expressed in in./μs. The trend indicated by C_{B22} for the three materials (the transverse shock wave travels fastest in S-Glass/Epoxy and slowest in Kevlar/Epoxy) is seen clearly in figure 2. A rough estimate of the normal wave velocity can be obtained by counting the number of elements that appear to be affected by the impact from figure 2. The normal wave velocity estimates from the 1 μs and 3 μs frames are shown below: (note that displacement propagation after 1 μs is not shown in fig. 2)

Composite system	Number of elements		Velocity		Average
	1 μs	3 μs	1 sec	3 sec	
S-Glass/Epoxy	10	25	0.1313	0.1094	0.1204
T-300/Epoxy	7	16	.0788	.0700	.0744
Kevlar/Epoxy	5	12	.0657	.0520	.0589

These values are in close agreement with the values predicted using equation (2) for C_{B22}. The same trend is also seen for the 3 and 5 μs frames. It can be concluded that the initial shock travels with the bulk wave velocity C_{B22} along the direction of impact.

Once the normal shock reaches the bottom of the beam, the wavefront appears to be moving in the longitudinal direction forming a flexural wave. The velocities of the waves traveling in the longitudinal direction can be estimated with the same technique mentioned earlier. The following are the details for the frame after 13 μs (not shown in fig. 2).

Composite system	Number of elements	Velocity, in./μs
S-Glass/Epoxy	11	0.0510
T-300/Epoxy	9	.0416
Kevlar/Epoxy	7	.0320

The above velocities have the same trend as the bulk shear wave velocity parameter C_{S12}. However, the waves propagating in the longitudinal direction appear to move significantly slower than the calculated shear wave velocity. This is probably due to the coupling between the flexural wave and the shear wave. The flexural wave velocity is significantly slower than the shear wave velocity. For example, the smooth S-Glass/Epoxy specimen has a flexural wave velocity C_F given by

$$C_F = 2Pf = 0.0137 \text{ in./μs}$$

where P is the length between the supports and f is the first fundamental frequency. It is assumed that the wave number is 1 and the beam deflects into a half wave.

Static and dynamic stress contours. - The static and dynamic stress contours for notched S-Glass/Epoxy specimen are shown in figure 3. They appear to be identical. The peak values for the dynamic load case, however, are slightly lower than those for the static case. Steep stress gradients are observed near the load application point and at the notch tip. It is seen that all the three stresses attain very high peaks, indicating severe local stress intensities near the notch-tip. As the stress allowables for σ_{22} and σ_{12} are generally an order of magnitude lower than that for σ_{11}, one can except a matrix initiated failure followed by fiber fractures at this location.

Free-Edge Stress Analysis of Composite Laminates

Specimen geometry and finite element idealization. - The geometry of the laminated plate under study and the finite element mesh employed for the primary and superelement structures are shown in figure 4.

One element is used through the thickness of each layer. There are 7 elements across the plate width and 28 elements along the plate length. A total of 1365 brick elements are used to model the primary structure. The superelement contains 224 elements with progressively decreasing mesh size toward the free edge. With this type of arrangement, the center of the element nearest

to the edge is 1/512 in. from the edge. The boundary conditions imposed are such that along the edge $x = 0$ every node in the midplane is constrained from displacements in x, y-, and z-directions. Also, the rest of the nodes along the edge $x = 0$ are constrained from displacement in the x-direction. Along the edge $x = 28$ in. a uniform stress of magnitude unity is prescribed.

Cases investigated. - The types of laminates investigated in the present study are $(\pm 10)_S$ through $(\pm 80)_S$ at 10° intervals. The $(\pm 45)_S$ laminate is also studied as a special case since it has been given substantial attention in the literature. The interply layers are assumed to be isotropic with $E = 0.5$ mpsi and $\nu = 0.35$. These are representative properties of an epoxy matrix. The thickness of the interply layer is taken as 0.000067 in. The plies are assumed to be homogeneous and orthotropic. The material properties chosen for the plies are typical of an AS-graphite fiber/epoxy composite system and are generated using, ICAN (ref. 7). The details are described in reference 2.

Free-edge stress. - In order to study the three-dimensional stress behavior near the straight free edge, a small region close to edge is isolated and modeled as a substructure (superelement). This region is shown in figure 4. Typical results for a $(\pm 10)_S$ AS-graphite/epoxy laminate are shown in figure 5. The six stresses, which were obtained near the free-edge region, are summarized in figure 5. These results are plotted against a length parameter X_f along a central line perpendicular to the free edge. The length parameter X_f is related to the distance from the free edge L_f (fig. 4) by

$$X_f = 1 - L_f \tag{4}$$

In the figure the dashed lines represent the stress computed at the center of $(\pm\theta)$ ply elements. The solid lines represent the stress computed at the center of the interply layer between $(+\theta)$ and $(-\theta)$ layers. The stresses are normalized with respect to the applied stress $\sigma_{xx\infty}$. The classical laminate analysis predictions for these normalized stresses are

$$\frac{\sigma_{xx}}{\sigma_{xx\infty}} = 1; \qquad \frac{\sigma_{yy}}{\sigma_{xx\infty}} = 0 \tag{5}$$

Inplane stresses σ_{xx}, σ_{xy} and σ_{yy}. - The inplane stresses σ_{xx}, σ_{xy}, and σ_{yy} approach classical laminate theory predictions in the interior of the ply. Close to the free edge, however, significant changes in these stresses are clearly seen. The transverse normal stress σ_{yy} in the $+\theta$ ply appears to be negligible. However, it does not vanish because of the presence of the interply layer. The maximum σ_{yy} observed in the $+\theta$ ply is less than 10 percent of the applied stress. The σ_{xy} stress in the interply layer is negligible and can not be seen distinctly. Both σ_{xy} and σ_{xx} in the $+\theta$ ply are seen to approach a finite value near the edge. A sign reversal is observed for these stresses.

Interlaminar stresses σ_{xz}, σ_{zz}, and σ_{zy}. - The interlaminar shear stress σ_{xz} has the greatest magnitude among these stresses. A steep increase in magnitude is seen near the free-edge zone. The stress magnitude in the interply layer is higher than that of the $+\theta$ ply. The interlaminar normal stress σ_{zz} appears to be of minor significance. However, it does have a definite trend. Two sign reversals are clearly noted. It starts as a compressive stress in the

interior of the ply or the interply layer, becomes a tensile stress for a short distance closer to the edge, and then reverts to a compressive stress near the edge. The maximum σ_{zz} observed is about 3 percent of the applied stress.

Effect of width to thickness ratio on interlaminar stress peaks. - A limited study with (±45) symmetric laminate has been conducted to assess the effect of width to thickness ratio on the interlaminar stress peaks. The stresses σ_{xz} and σ_{zz} are selected for the study because they appeared to be the only significant interlaminar stresses. The results are shown in figure 6. The stresses are computed 3/512 in. from the free edge. Four ratios of W/h, where W is the and h is the thickness, are chosen in the study. The results show significant sensitivity to the W/h ratio. Both stresses appear to have substantial magnitudes for the laminate with W/h = 8. As the laminate becomes thinner, however, σ_{zz} appears to reach a zero value while σ_{xz} continues to have a significant magnitude.

Fracture Toughness Predictions of Composites for Individual and Combined Fracture of Modes I, II, III.

Geometry and finite element idealization. - The three point bend test specimens for end notch flexure (ENF) and mixed mode flexure (MMF) are used in the finite element evaluation of the fracture toughness for composites. These tests have been the subject of discussion and evaluation of ASTM D30.02 and D30.04 subcommittee meetings and specialty symposia sponsored by their subcommittees (ref. 3). Figure 7 describes the geometry and figure 8 shows the details of the finite element model with the crack-tip superelement.

A line load was applied at the specimen midspan. The magnitude of this load was 120 lb. This magnitude corresponds to the experimental load which induced unstable crack propagation (ref. 3). The crack extension propagation was simulated by progressively deleting interply layer elements and repeating the FEA as described in reference 4.

The composite material simulated was AS-graphite fiber/epoxy matrix (AS/E) unidirectional composite. The unidirectional ply properties, the interply layer thickness and its properties, and the appropriate material properties required for the three-dimensional finite element analysis were generated with the aid of ICAN (ref. 7). The properties for the interply layers were assumed to be the same as those for the matrix. The specific values for the three-dimensional composite properties (using MSC/NASTRAN designation) and interply layer thickness predicted by ICAN are described in reference 3.

RESULTS AND DISCUSSION

The modes II SERR (strain energy release rate), using the local crack closure method (ref. 3), is shown in figure 9 (dashed line) for 0.6 FVR. The curve determined using the global method is also plotted for comparison. The range of limited experimental data (ref. 3) is shown by dashed horizontal lines. Three points are worth noting in figure 9:

(1) The global method predicts higher G_{II} values than the local crack closure method.

(2) The two methods predict similar composite interlaminar fracture behavior.

(3) A conservative assessment of the composite interlaminar fracture characteristics can be obtained by using the G_{II} determined from the local crack closure method.

The mixed mode (I and II) composite interlaminar fracture characteristics, determined from the local crack closure method, are shown in figure 10 for a composite with 0.6 FVR. The fracture characteristics for each mode (mode I and II) are compared with those predicted for the mixed mode by using the global method (solid line) and the algebraic sum of the two modes from the local method (short dashed line). The following observations are worth noting in figure 10:

(1) Both the local crack closure and the global methods predict similar mixed mode (mode I and II) fracture characteristics.

(2) The local crack closure method predicts lower mixed mode G values than the global method.

(3) Mode II fracture dominates the crack extension during slow and stable crack growth ($a < 1.05$ in.).

(4) Mode I dominates the crack extension during unstable crack growth and rapid crack propagation ($a > 1.15$ in.).

The general conclusions to be drawn from the above observations are:

(1) The contribution of each fracture mode can be determined using the local crack closure method.

(2) Mode I drives the composite interlaminar delamination in MMF specimens.

(3) The local method provides a conservative assessment of mixed mode composite interlaminar fracture characteristics as was the case for mode II.

Mixed Modes I, II, and III in Composite Laminates

The computational procedure described in reference 3 has been modified to determine mixed modes I, II, and III in composite laminates (ref. 4). The laminate configurations used in these studies were unbalanced, and unsymmetric $[-\theta_m/+\theta_n]$. These laminates were selected in order to evaluate the effects of the different laminate material-coupling coefficients. in the laminate force deformation relationships, on the individual and mixed mode fracture strain energy release rates (SERR).

The specific laminates $(-\theta_{36}/+\theta_{12}]$, $\theta = 0°$, 15°, 30°, 45°, 60°, 75°, and 90°) were investigated for the laminate configuration effects on the SERR. At the $\theta = 45°$ position, a total of three cases ($[-45_m/45_{12}]$, m = 36, 60, and 84) were investigated for the interlaminar crack location effects on SERR. It is important to note that these specific laminate configurations and the

interlaminar crack locations were selected only for computational simulation convenience. They represent just one application of the present procedure.

Effects of Ply Orientation

The effects of ply orientation on the maximum individual and mixed mode fracture SERR (assuming a 480 lb load) are plotted in figure 11 for the seven cases of the $[-\theta_{36}/+\theta_{12}]$ (θ = 0°, 15°, 30°, 45°, 60°, 75°, and 90°) AS/E laminate. The relative dominance of the opening fracture mode SERR (G_I) and the negligible contribution of the tearing fracture mode SERR (G_{III}), on the maximum mixed fracture mode SERR (G_T) are clearly observed in this figure. Another observation is that the "maximum" magnitude of mixed mode fracture (G_T) levels off at ply angle orientations greater than 60°.

The above observations lead to the following conclusions: (1) the rapid or unstable interlaminar crack growth is dominated by the opening fracture mode; (2) the tearing fracture mode SERR (G_{III}) is negligible compared to G_T for ply orientation angles greater than 60°; (3) the individual fracture modes (G_I and G_{II}) and the mixed mode fracture are practically independent of ply orientation angle greater than 60°; and (4) ply orientation angles less than 60° have significant influence on the SERR of individual fracture mode and mixed mode fracture.

Effects of Laminate Configuration

The effects of the laminate configuration on the SERR due to a 480 lb load are also shown in figure 11. The effects on the individual fracture mode SERR's are plotted in figure 11(a) to (c). The SERR for the mixed fracture mode (G_T) is plotted in figure 11(d). The important observations in this figure are: (1) the shearing mode fracture SERR (G_{II}) appears to reach a maximum and then decrease with increasing crack opening for practically all the laminate configurations, (2) the tearing mode fracture SERR (G_{III}), on the other hand, continues to increase with crack length for some laminate configurations.

The conclusion from the above discussion is that laminate configurations can be selected for "stable" shearing and tearing fracture mode crack growth for given composite components and loadings. It is important to keep in mind that advantages of this can be taken only in the absence of opening mode fracture.

SUMMARY OF RESULTS

The significant general and specific conclusions of the present investigation are listed below:

General Conclusions

1. Finite element substructuring methods are computationally effective in dealing with the issues related to singular/near singular stress fields encountered in advanced composite structures.

2. These methods are used at NASA Lewis Research Center to analyze a variety of problems of current interest to the composites community.

3. The results indicate the versatility of the finite element substructuring methods in the computational simulation of the complex composite singularity problems.

Specific Conclusions

1. The wave propagation velocities can be estimated from the early time displacement propagation response,. the estimates are in fair agreement with the theoretical predictions.

2. The dynamic and static peak load stress contours are almost identical. The static peak load stress magnitudes are slightly higher. Stress predictions based upon a quasi-static approach lead to conservative estimates.

3. The notch-tip region develops severe stress concentrations and any of the three stresses could cause or initiate a failure.

4. The interlaminar stresses σ_{xz}, σ_{zz}, and σ_{zy} are of second order compared to σ_{xx} in general. However, the interlaminar shear stress σ_{xz} could become substantial in the interply layer free-edge region depending on the configuration of the angleply laminate.

5. Progressive mesh refinement is an effective way to describe the behavior of the interlaminar stresses as the free edge is approached. The results indicate stable convergence of these stresses with some noise as the free edge is approached.

6. The magnitudes of the interlaminar stress peaks are sensitive to the width to thickness ratio of the laminate. Results obtained from relatively narrow specimens are not indicative of practical laminate behavior.

7. The individual and mixed mode fracture SERR can be readily determined using a computational simulation procedure that consists of three-dimensional finite element analysis and integrated composite mechanics.

8. Individual and mixed mode fracture SERR magnitude of $[-\theta_m/+\theta_n]$ are strongly influenced by crack length, ply angle, and interlaminar crack location. However, the maximum magnitude of the mixed mode fracture SERR (G_T) is practically independent for ply orientations greater than 60°

9. The tearing fracture mode SERR (G_{III}) has the smallest magnitude compared to opening (G_I) and shearing (G_{II}) fracture modes for this case. The tearing fracture mode is generally present in combinations with other fracture modes.

10. Stress magnitudes ahead of the crack tip can be compared with corresponding local laminate strengths in order to determine the dominant stress which drives the crack.

11. Collectively the results demonstrate that the procedure described herein can be used to computationally simulate/evaluate mixed mode fracture toughness parameters in composite components subjected to complex loadings.

REFERENCES

1. Murthy, P.L.N.; and Chamis, C.C.: Dynamic Stress Analysis of Smooth and Notched Fiber Composite Flexural Specimens. Composite Materials: Testing and Design, ASTM STP 893, J.M. Whitney, ed., American Society for Testing and Materials, 1986, pp. 368-391. (NASA TM-83694).

2. Murthy, P.L.N.; and Chamis, C.C.: A Study of Interply Layer Effects on the Free Edge Stress Field of Angleplied Laminates. Comp. Struct., vol. 20, no. 1-3, 1985, pp. 431-441. (NASA TM-86924).

3. Murthy, P.L.N.; and Chamis, C.C.: Interlaminar Fracture Toughness: Three-Dimensional Finite Element Modeling for End-Notch and Mixed-Mode Flexure. (NASA TM-87138), 1985.

4. Murthy, P.L.N.; and Chamis, C.C.: Composite Interlaminar Fracture Toughness 3-D Finite Element Modeling for Mixed Mode I, II, and III Fracture," (NASA TM-88872), 1986.

5. Newmark, N.M.: Method of Computation for Structural Dynamics. J. Eng. Mech. Div., Am. Soc. Civ. Eng., vol. 85, no. EM-3, pt. 1, July 1959, pp. 67-94.

6. MacNeal, R.H.: The NASTRAN Theoretical Manual, (Level 15.5). MacNeal-Schwendler Corp., 1972.

7. Murthy, P.L.N.; and Chamis, C.C.: Integrated Composite Analyzer (ICAN): Users and Programmers Manual, NASA TP-2515, 1986.

ORIGINAL PAGE IS
OF POOR QUALITY

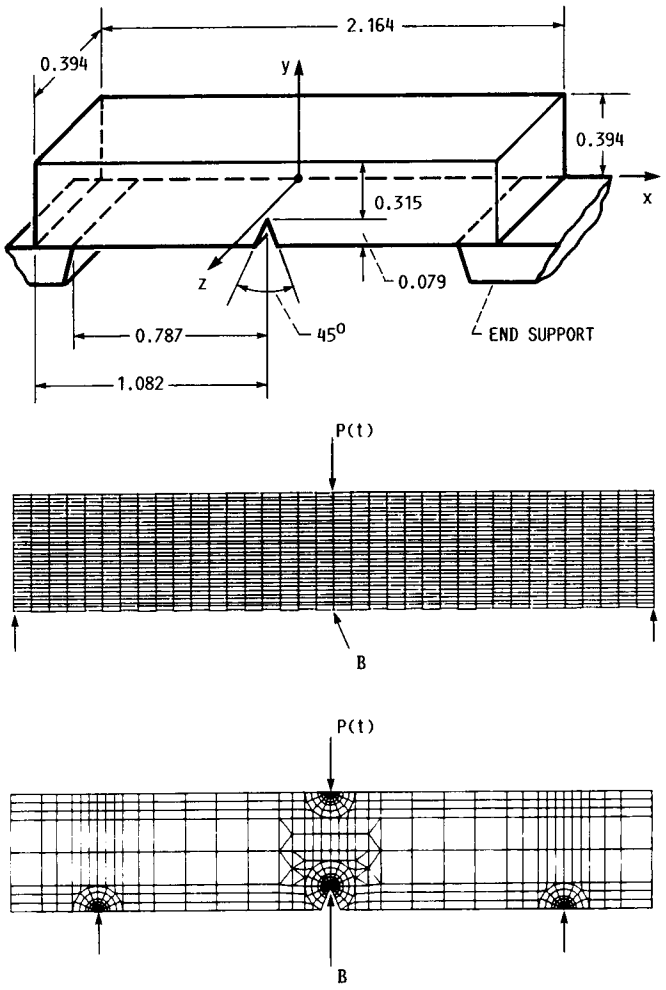

FIGURE 1. - ASTM CHARPY TEST SPECIMEN AND FINITE ELEMENT IDEALIZATION OF SMOOTH AND NOTCHED SPECIMENS.

DISPLACEMENT PROPAGATION

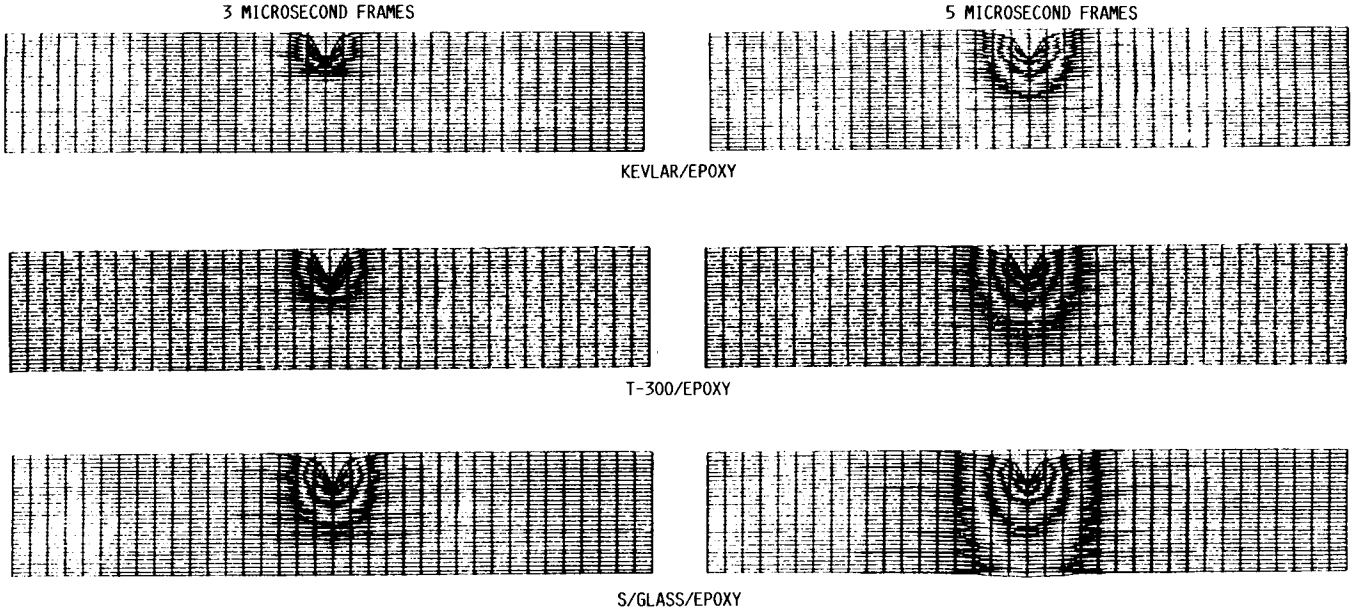

FIGURE 2. - DYNAMIC DISPLACEMENT PROPAGATION IN THE THREE COMPOSITE SYSTEMS SELECTED AFTER 3 μs AND 5 μs.

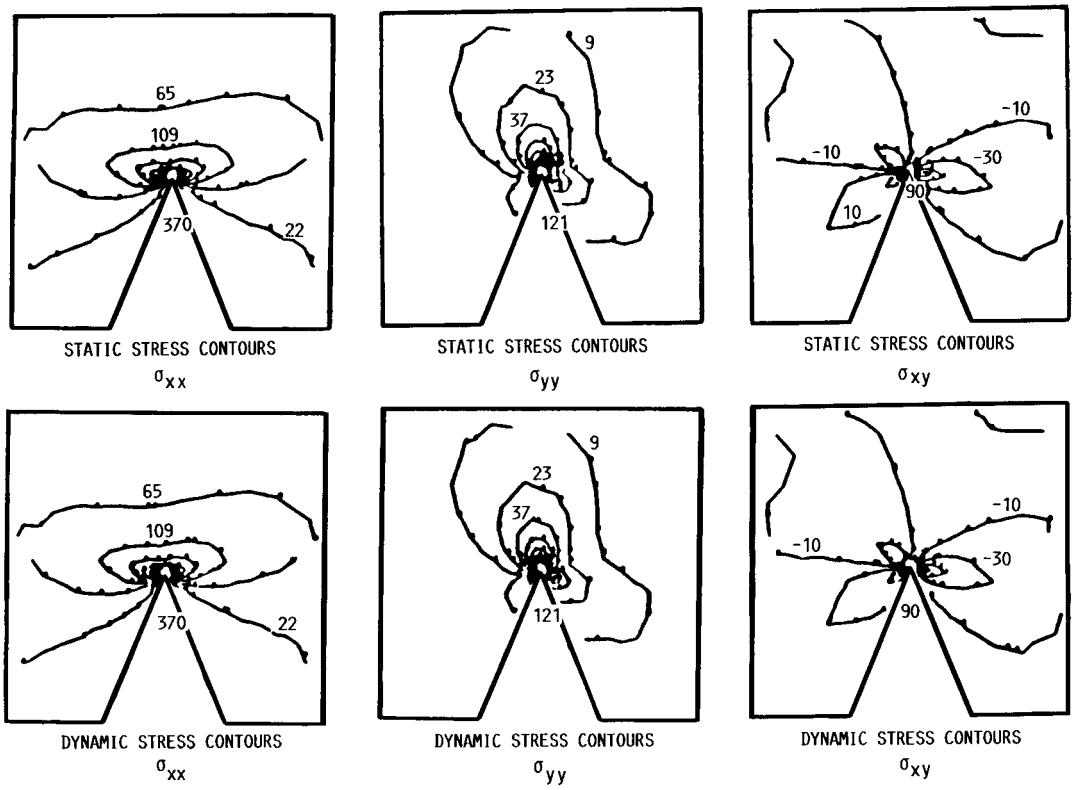

FIGURE 3. - DYNAMIC/STATIC STRESS CONTOURS NEAR THE NOTCH REGION AT PEAK LOAD FOR S-GLASS/EPOXY NOTCHED FLEXURAL SPECIMEN.

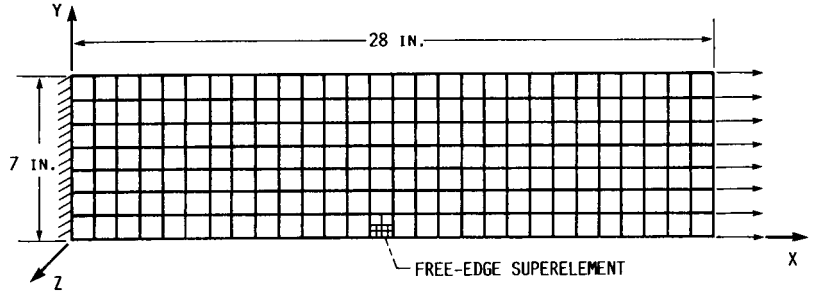

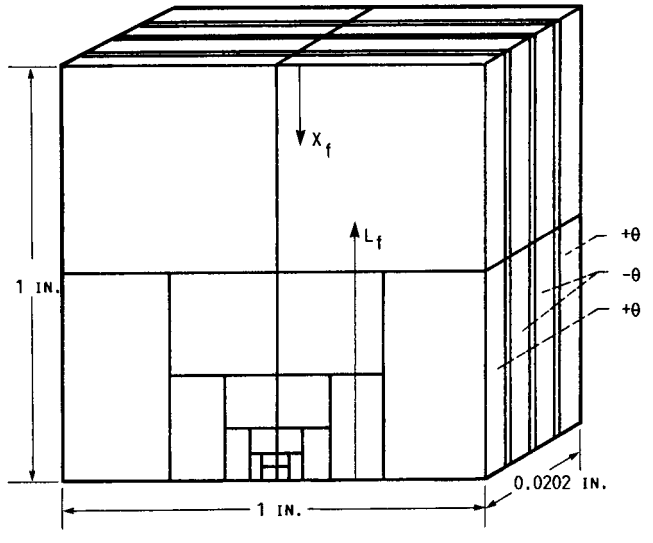

FIGURE 4. - ANGLEPLIED LAMINATED PLATE GEOMETRY AND THE FINITE ELEMENT IDEALIZATION.

ORIGINAL PAGE IS
OF POOR QUALITY

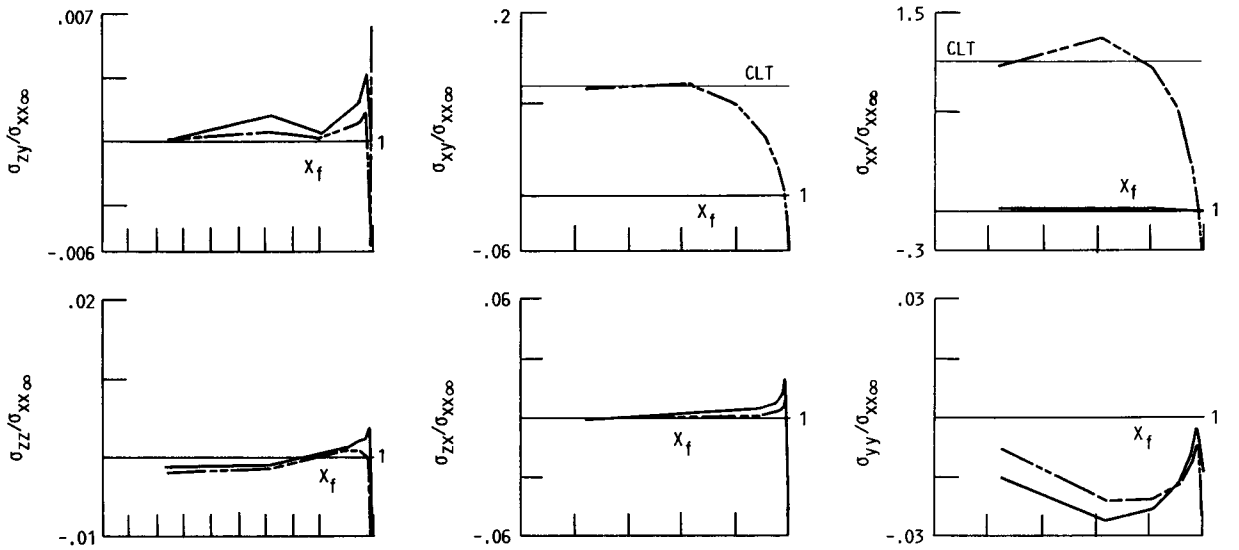

FIGURE 5. - FREE-EDGE STRESSES IN $+10^0$ AND INTERPLY LAYERS OF (±10) LAMINATE. (SOLID CURVE, INTERPLY LAYER; DASHED CURVE, CNETER OF THE PLY).

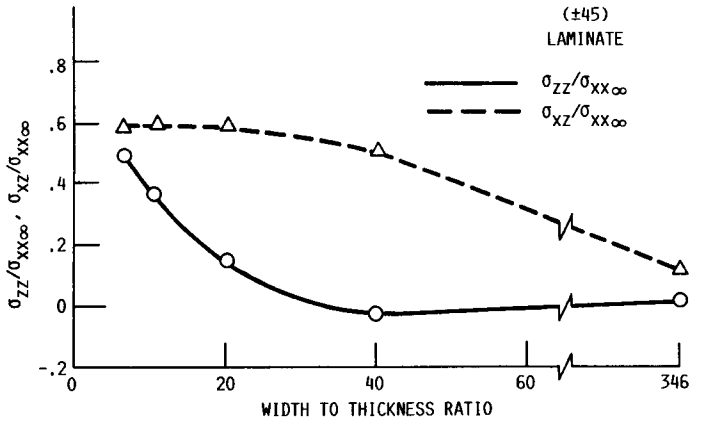

FIGURE 6. - WIDTH TO THICKNESS RATIO EFFECTS ON INTERLAMINAR STRESSES σ_{xz} AND σ_{zz} FOR A $(\pm 45)_s$ AS GRAPHITE/EPOXY LAMINATE.

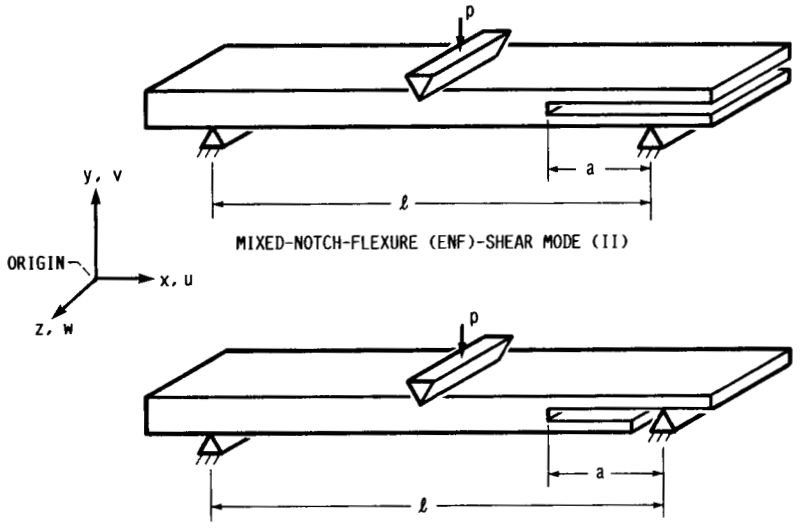

FIGURE 7. - SCHEMATIC OF FLEXURAL TEST FOR INTERLAMINAR FRACTURE MODE TOUGHNESS.
NOTE: ORIGIN AT LEFT SUPPORT BOTTOM.

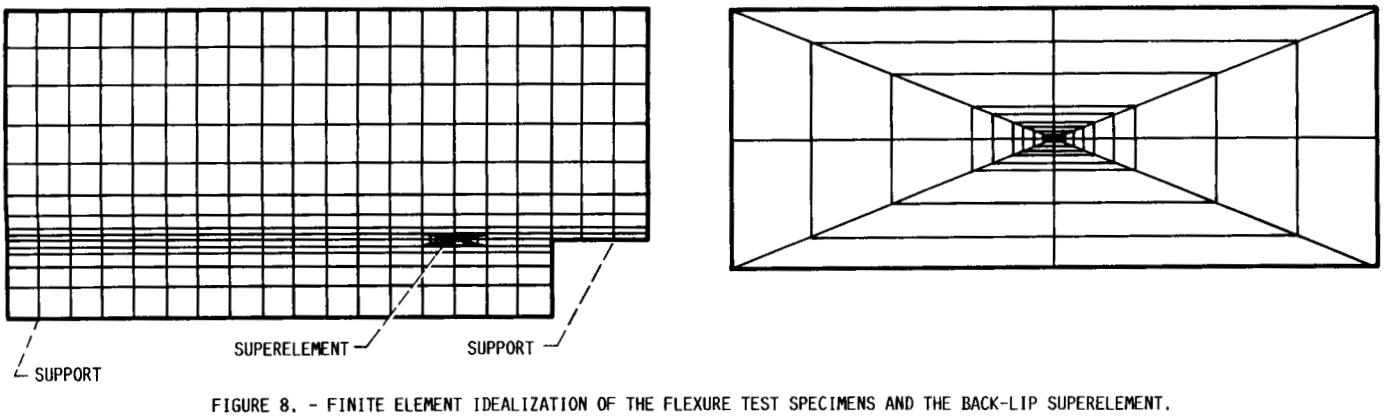

FIGURE 8. - FINITE ELEMENT IDEALIZATION OF THE FLEXURE TEST SPECIMENS AND THE BACK-LIP SUPERELEMENT.

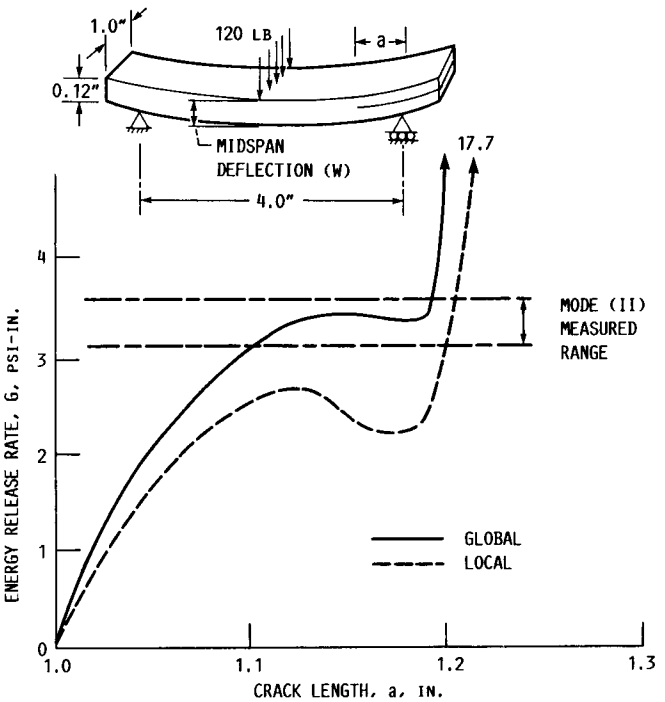

FIGURE 9. - END-NOTCH FLEXURE ENERGY RELEASE RATE COMPARISON.

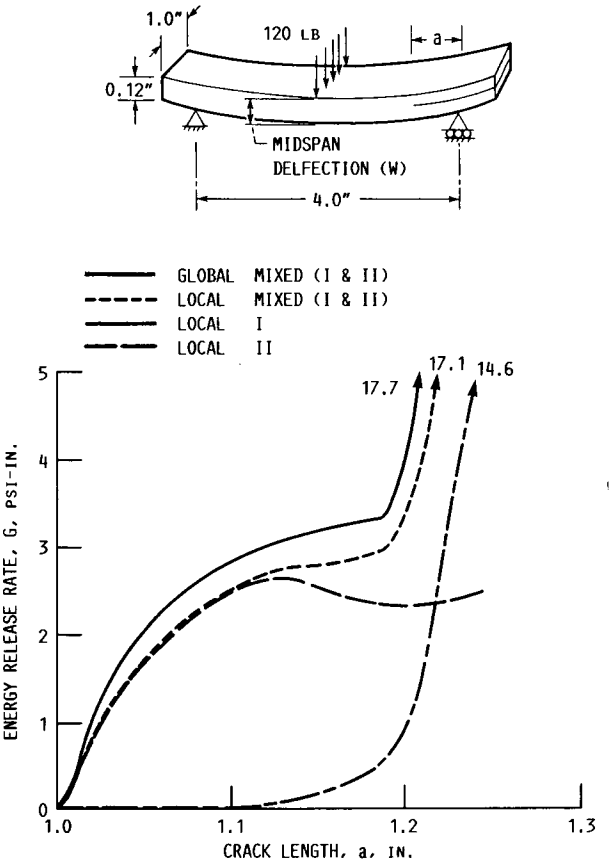

FIGURE 10. - MIXED-MODE-FLEXURE ENERGY RELEASE RATE AND COMPONENTS (AS/E). LOCAL CLOSURE METHOD.

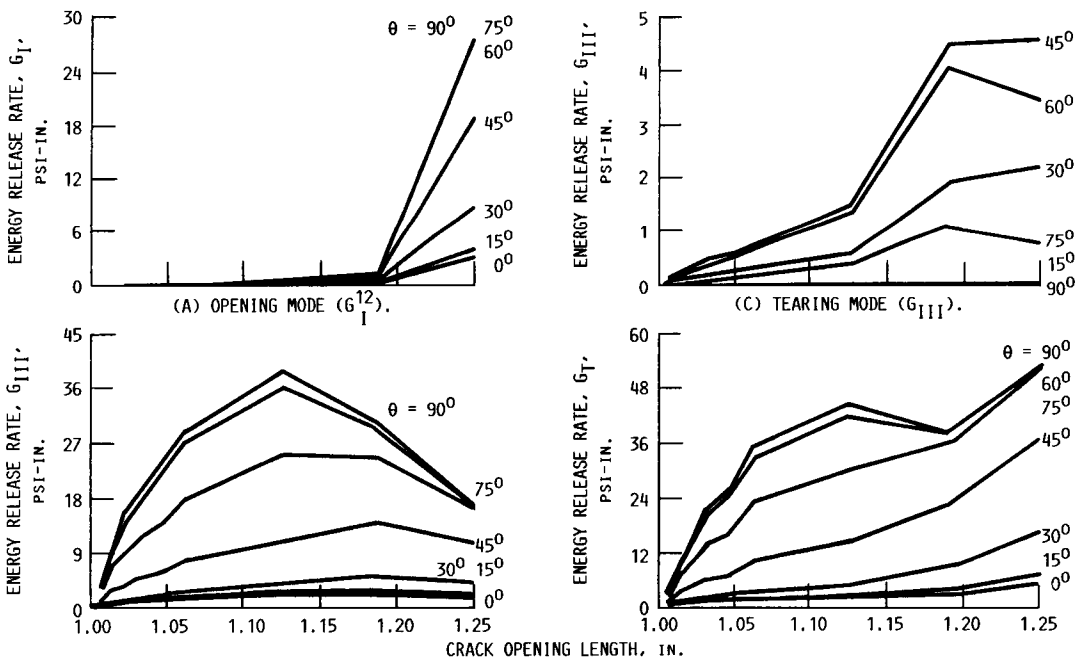

FIGURE 11. - EFFECT OF LAMINATE CONFIGURATION ON STRAIN ENERGY RELEASE RATES ($[-\theta_{36}/+\theta_{12}]$; AS/E WITH 0.6 FVR).

NASA
National Aeronautics and Space Administration

Report Documentation Page

1. Report No.	2. Government Accession No.	3. Recipient's Catalog No.
NASA TM-100297		

4. Title and Subtitle	5. Report Date
Finite Element Substructuring Methods for Composite Mechanics	6. Performing Organization Code

7. Author(s)	8. Performing Organization Report No.
Pappu L.N. Murthy and Christos C. Chamis	E-3946
	10. Work Unit No. 505-63-11

9. Performing Organization Name and Address	11. Contract or Grant No.
National Aeronautics and Space Administration Lewis Research Center Cleveland, Ohio 44135-3191	13. Type of Report and Period Covered Technical Memorandum

12. Sponsoring Agency Name and Address	14. Sponsoring Agency Code
National Aeronautics and Space Administration Washington, D.C. 20546-0001	

15. Supplementary Notes

Prepared for the International Conference on Composite Materials and Structures, sponsored by the India Institute of Technology at Madras, Madras, India, January 6-9, 1988. Pappu L.N. Murthy, Cleveland State University, Civil Engineering Department, Cleveland, Ohio 44115; Christos C. Chamis, NASA Lewis Research Center.

16. Abstract

Finite element substructuring strategies to obtain numerical solutions for three typical problems of interest to the composites community, are presented in this paper. The key issue common to these problems is the presence of singular or near singular stress fields. The regions prone to see steep stress gradients, are substructured with progressively refined meshes to study the local response simultaneously with the global response. The results from the select examples indicate that finite element substructuring methods are computationally effective for composite singularity mechanics.

17. Key Words (Suggested by Author(s))	18. Distribution Statement
Fiber composites; Stress wave propagation; Fracture toughness; Free edge stresses; Delamination; Substructure; Interply layer; Interlaminar fracture; Mode I; Mode II; Mode III; Mixed-mode fracture; Strain energy release rate composite mechanics; Transient response; Superelement	Unclassified - Unlimited Subject Category 24

19. Security Classif. (of this report)	20. Security Classif. (of this page)	21. No of pages	22. Price*
Unclassified	Unclassified	16	A02

*For sale by the National Technical Information Service, Springfield, Virginia 22161